Renewable and Sustainable Energy Reviews 14 (2010) 2926–2935

Contents lists available at ScienceDirect

Renewable and Sustainable Energy Reviews

journal homepage: www.elsevier.com/locate/rser

Analysis of spectrum distribution and optical losses under Fresnel lenses

Naichia Yeh *

School of Applied Sciences, MingDao University, 369 Wen Hua Road, Peetou, Changhua 52345, Taiwan, ROC

ARTICLE INFO

Article history:
Received 11 May 2010
Accepted 14 July 2010

Keywords:
Device modeling
Fresnel lens
Solar concentrator

ABSTRACT

During late 1970s and early 1980s, Fresnel lenses have received more attention in the field of solar energy application. This paper briefly examines the Fresnel lens development since 1970s and investigates the losses inherent in the linear Fresnel lenses. The research develops the formulation that helps to quantify the linear lens' transmittance loss and prism-tip scattering loss and then derive a realistic model to simulate the measured data. In addition, the research has identified an elliptical-based lens that comes closest to the condition of minimum deviation. Such lens closely duplicates the curvature needed for maximum transmission. The researcher applies different design wavelengths to study the contribution of each wavelength interval on the receiving plane.

Contents

1. Fresnel lens development

The Fresnel lens was invented in 1822 by a French mathematician and physicist, Augustin Jean Fresnel. The invention was based on the long-known fact that the contour of refracting surfaces (rather than the material in between) of a conventional lens defines its focusing properties. The material between these two surfaces only increases the lens' absorption losses. In a linear Fresnel lens the bulk is reduced by the extraction of a set of parallel grooves of material to form a set of inclined surfaces (Fig. 1, right). Near the lens centerline, these inclined serrations are nearly parallel to the plane face; toward the outer edge, the inclined surfaces become steeper. The inclined surface of each serration is the corresponding portion of the original aspheric surface. The angle of each serration is modified slightly from that of the original aspheric profile to eliminate spherical aberration.

The first Fresnel lenses are flat lenses. The incident angle of flat lenses is always zero, which induce no refraction. And thus large second face incident angles are needed to fulfill all the refraction need. Cosby [1] and Hasting et al. [2,3] have found that the optical performance of the Fresnel lens improves when its base is curved rather than flat. Flat lenses that have large second face incident angles have much poorer performance than those with small second face incident angles because different spectrum segments would spread when passing through a lens and cause *chromatic aberration*. As the incident angle of the second face approaches $\sin^{-1}(1/\tilde{n})$, the spread becomes larger and part of the flux tends to miss the designated target area. In addition, an incident angle greater than $\sin^{-1}(1/\tilde{n})$ would result in total internal reflection (TIR), which blocks the flux from penetrating the lens. James and Williams [4] have concluded that total internal reflection can be reduced as more refraction takes place on the first surface and less on the second surface of the lens. Such condition also reduces chromatic aberration and allows the use of smaller cells, which leads to lower system cost. A curved-base lens has more design freedom for the curvature of its first face can be treated as a design parameter to cut its dependency to greater second face incident angles.

Two classes of Fresnel lenses have evolved since 1970s. They include O'Neill's concentration point-focusing lens [5,6] and Kritchman et al.'s nonimaging lens [7,8]. Point-focusing lenses

* Tel.: +886 4 887 6660x8114; fax: +886 4 887 6661.
E-mail address: nyeh@mdu.edu.tw.

1364-0321/$ – see front matter © 2010 Elsevier Ltd. All rights reserved.
doi:10.1016/j.rser.2010.07.016

Nomenclature

E_{mn}	n^{th} wavelength interval of incoming solar radiation that goes through the m^{th} facet
l	the width of each prism tip (the tip width is independent of the prism width)
M	total number of facets on the lens
N	number of wavelength intervals applied to the model
R	combined loss caused by factors such as TIR, blocking, surface reflectance, and scattering due to groove defects and distorted lens material
T_{mn}	transmittance coefficient of the solar radiation within n^{th} wavelength interval on the m^{th} facet
T_{mn_1}	entry face transmission factor
T_{mn_2}	exit face transmission factor
T_s	tip scattering loss
$\tilde{n}_n$	refractive index of the lens material for the n^{th} wavelength interval
θ	facet angle, the angle between the prism's entry face (AB) and exit face (AC)
θ_v	complement of face angle with respect to the optical axis
φ_i	incoming radiation's entry face incident angle
φ_r	refraction angle of the incident ray on face AB
φ_r'	exit face (AC) refraction angle
η	side angle, the angle between face AB and the prism's side face (BC)
δs_m	width of m^{th} facet
φ_{mn_i}	entry face incident angle of n^{th} wavelength interval at the m^{th} facet
φ'_{mn_i}	exit face incident angle of n^{th} wavelength interval at the m^{th} facet
φ_{mn_r}	exit face incident angle of n^{th} wavelength interval at the m^{th} facet
φ'_{mn_r}	exit face the incident angle of n^{th} wavelength interval at the m^{th} facet

need to operate in normal incidence with accurate sun tracking, while a nonimaging lens does not focus on one focal point to create an image. Nonimaging lenses are intended for solar energy collection. As long as the lens captures radiation, its photographic accuracy is of little concern. The nonimaging lenses use the edge ray principle introduced by Winston [9] and Rabl [10] for compound parabolic concentrators (CPC). The edge ray principle describes a condition in which radiation entering the system within the boundaries of the edge rays (or called extreme ray) exits the system within the boundaries of the exiting edge rays. For maximal optical concentration, the extreme rays entering through a lens surface must be extreme rays exiting the system through receiver. When this concept is applied to a nonimaging Fresnel lens, the facets on the lens are constructed so that the edge ray entering the lens surface is refracted to the absorber at a segment instead of at one point.

Cosby [11] pointed out that the required target width of a Fresnel lens concentrator generally decreases and peak concentration value increases with increasing lens curvature. In order to vary the curvature of the lenses with respect to their focal plane, Cosby used circular sections with radii at points above or below the focal plane.

Collares-Pereira et al. [12,13], among other researchers, have proposed secondary concentrators to correct the focal aberrations inherent in a Fresnel lens system.

Lorenzo and Luque [14,15] and Lorenzo [16] have used different approaches to give thorough analyses of Fresnel lenses for solar concentration. They have found that lenses with elliptical shapes have some interesting properties. One of the shapes almost exactly duplicates the curvature required to achieve maximum transmission. When the flux's first face incidence angle equals its refraction angle from the second face (i.e. when the ratio of incidence angle to refraction angle = 1), *minimum deviation* occurs. *Minimum deviation* condition is for maximum transmission of a prism and has been used in the design of prism spectrometers for years. While the importance of the maximum transmission is obvious, the minimum deviation means that small changes in the prism angles and positioning has the minimum possible effect on the turning angle of the light refracted from that prism. Errors in manufacturing and in the construction of systems are thereby minimized while the focusing capability of the lens maximized.

For linear focus Fresnel lens, Leutz et al. [17] have introduced a pair of acceptance angles, which are perpendicular to each other, that offset some daily and seasonally sunlight tracking error to refract maximum incident rays to the absorber. Yeh [18] has used optical geometry to derive a complete set of ray-tracing equations for an elliptical-based Fresnel lens concentrating system. To avoid the unpredictable factors that can induce complication in lens design, Yeh's model has assumed an ideal system in which the heights of the serrations are negligible. The extreme rays of the entry aperture are passing the optical system's exit aperture likewise as extreme rays. The amount of the radiation obstructed has thus been neglected. However, some loss factors inherited by the Fresnel lenses are unavoidable in the realistic lenses. These factors include total internal reflection, prism-tip scattering, and facet blocking. While some of the previous researches have discussed about a variety of inherent losses of the Fresnel lenses [19,20], the work to quantify such losses is still short. It is this paper's aim to investigate a more practical model which integrates TIR loss, facet blocking loss, reflectance loss, transmittance loss, and prism-tip scattering loss.

2. Tracking the loss

Trace the ray in Fig. 1 and apply Snell's law to obtain

$$(90-\theta)+\theta_v+\varphi_i-\varphi_r = 90-\varphi_r = 90-\sin^{-1}\left(\frac{\sin\varphi_i}{\tilde{n}_n}\right) \tag{1}$$

The incident ray between I and I' (beam I–I') has the best chance to reach the target area when:

$$\eta = 90-\sin^{-1}\left(\frac{\sin\varphi_i}{\tilde{n}_n}\right) \tag{2}$$

While greater η allows more light to reach face AC and then transmit through exit face to reach the target, it is also more likely to trigger the loss via blocking. That is, the incidence ray adjacent to the intersection of the two prisms (i.e. the left edge of beam I'–I'') is more likely to be blocked by face BC, the neighboring prism's side face. Contrastingly, a sharper η makes the left edge of beam $I'I''$ less likely to be blocked. Fig. 2 illustrates that a segment of beam II' does not refract toward face AC. Instead, the segment is refracted to face BC and trapped within the prism due to TIR when $\eta < 90-\varphi_r$.

Any refracted beam that hit one of the two tips in the prism (e.g. points C and D, as circled in Figs. 1 and 2) will be scattered and lost, disregard of the magnitude of η. This loss is called prism-tip

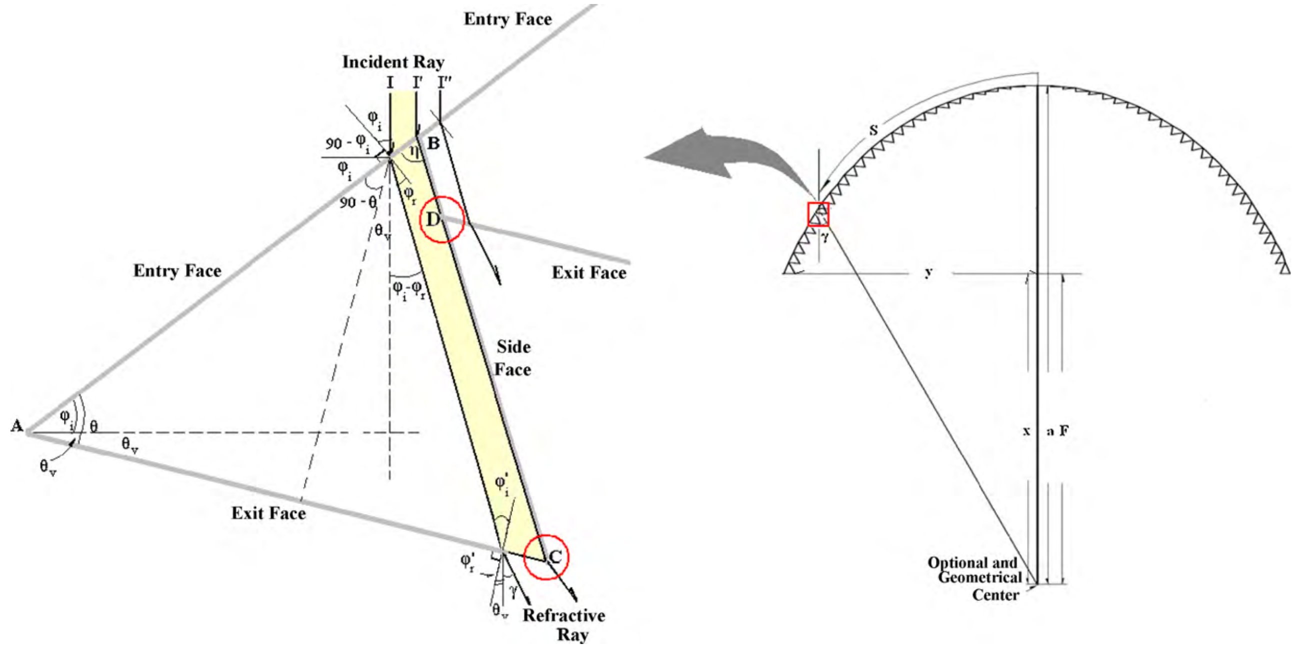


Fig. 1. Right: refraction of incident ray on a elliptical-based Fresnel lens with a focal ratio (i.e. the ratio of focal length to the lens aperture) of $x/2y$. Left: the diagram of two enlarged neighboring facets that depict the ray path into the entry face (AB), within the prism, and out of the exit face (AC).

scattering loss, which is defined as:

$$T_s = \frac{\text{The sum of the width of all tips}}{\text{The aperture of the entire lens}} = 2l\frac{M}{\sum_{m=1}^{M}\delta s_m} \quad (3)$$

Sharper prism tips can reduce the amount of scattering loss. However, due to the limitation of manufacturing workmanship, the tips are simply not able to reach the sharpness that can eliminate the tip scattering. While finer and denser prisms on the Fresnel lens can produce sharper images, the transmittance of the lens is sacrificed due to the increased number of the prism tips that producing scattering loss. Assume that the width of each tip is as fine as 0.03 mm each, a 300-facet lens will have 600 tips that make a total tip scattering width of 18 mm, which constitutes 6% of a 30 cm aperture lens. And a 200-facet lens that has 400 tips will contribute 12 mm to tip scattering loss.

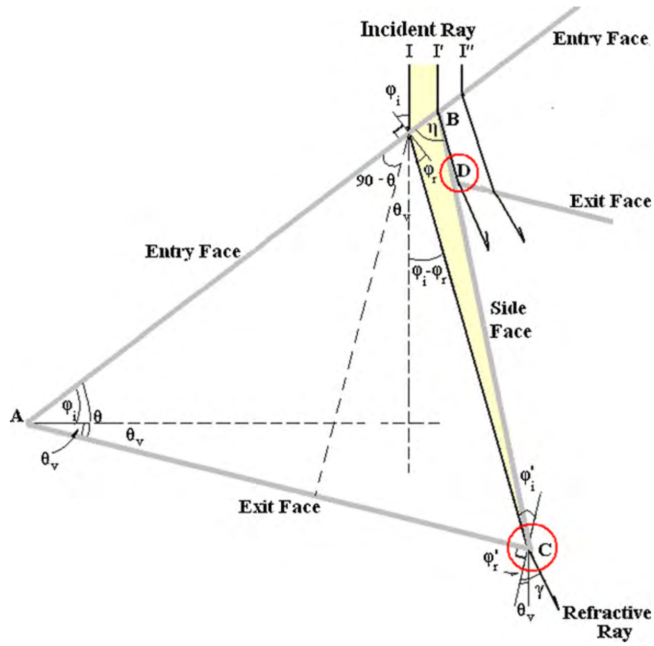


Fig. 2. Schematic for refraction of incident ray on two neighboring facets that depicts the ray path into the entry face (AB), within the prism, and out of the exit face (AC). The incidence between I and I' is blocked within the prism by the side face (BC) as shown.

Fig. 3 provides a more detailed look at TIR loss, blocking loss, and prism-tip scattering loss via different magnitudes of η. It is worth noticing that shorter wavelength is more inclined to TIR loss (as shown by beam I–I' at lens segment A) and longer wavelength is more apt to blocking loss (as shown by beam I'–I'' at lens segment B). For incidence I at the lens segment A, only the wavelength longer than red will reach the exit face after the entry face refraction. The light that has shorter wavelength will hit the side face (BC) in a large angle and get trapped within the lens due to TIR.

For incidence I' at the lens segment B, all the segments with wavelength not shorter than blue has the chance to reach the exit face after the first face refraction. The η can be adjusted to a magnitude so that no segment of the reflected spectrum would be blacked by the side face. However, as depicted by I'', all the segments with wavelength not shorter than red will be blocked after emitting the exit face. A greater η can only make such blocking loss worse.

The transmittance coefficient of the solar radiation within n^{th} wavelength interval on the m^{th} facet (T_{mn}) is the product of the entry face transmission factor (T_{mn_1}), the exit face transmission factor (T_{mn_2}), and the bulk transmission factor (T_b); less tip scattering loss (T_s) and the combined loss (R) that caused by factors such as TIR, blocking, surface reflectance, and scattering due to groove defects and distorted lens material. For a 3.2 mm thick acrylic, adding 2% of the combined loss is reasonable [18].

$$T_{mn} = T_{mn_1} T_{mn_2} T_b - T_s - R \quad (4)$$

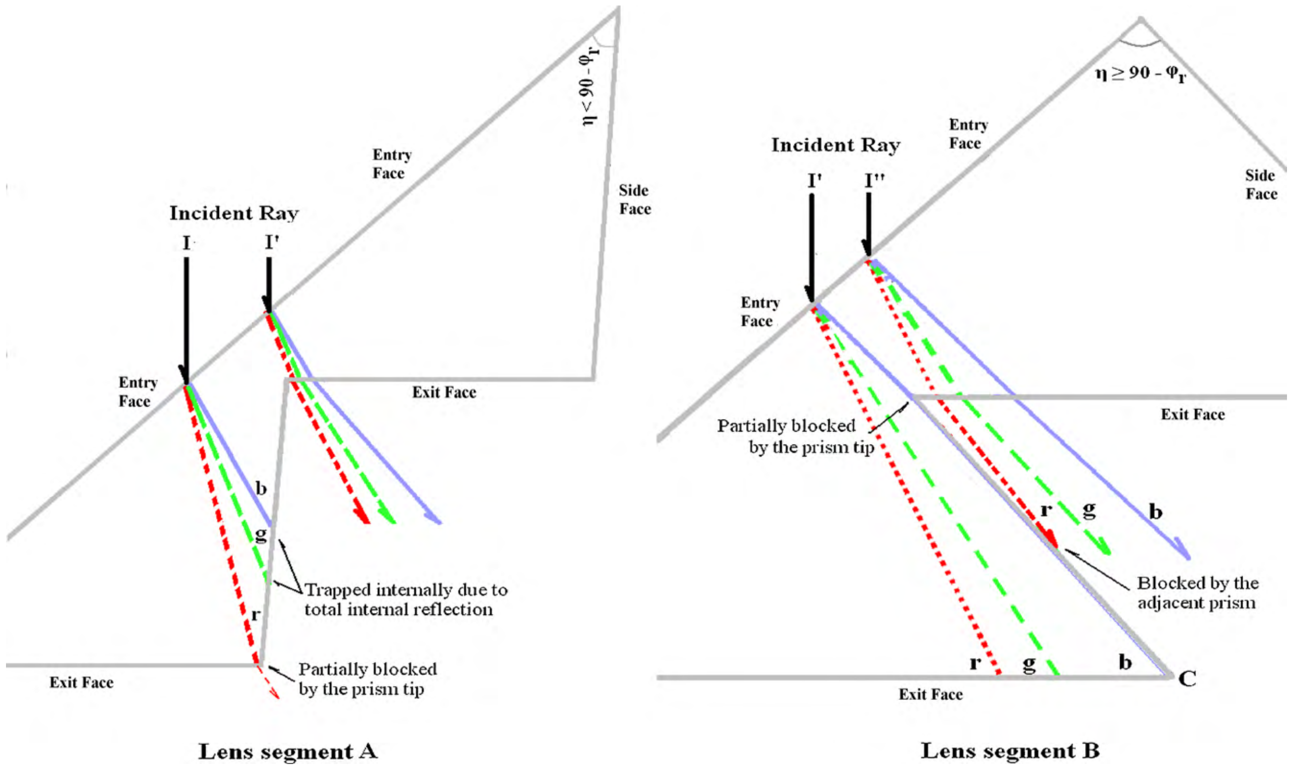


Fig. 3. Schematic of ray tracing through the facets on a curve-based Fresnel lens. The illustration inflates the light paths near the border of two adjacent facets in order to depict the loss caused by TIR, prism-tip scattering, and facet blocking. The facets that have small sharp η (lens segment A) are more inclined to TIR while having less tendency for facet blocking. On the contrary, a facet that has greater η (lens segment B) is more apt to facet blocking rather than TIR. For either case, prism-tip scattering is not avoidable.

T_{mn_1} and T_{mn_2} are, respectively [21],

$$T_{mn_1} = \frac{\sin(2\varphi_{mn_i})\,\sin(2\varphi_{mn_r})}{\sin^2(\varphi_{mn_i}-\varphi_{mn_r})}\left(1+\frac{1}{\cos^2(\varphi_{mn_i}-\varphi_{mn_r})}\right) \tag{5}$$

$$T_{mn_2} = \frac{\sin(2\varphi'_{mn_i})\,\sin(2\varphi'_{mn_r})}{\sin^2(\varphi'_{mn_i}-\varphi'_{mn_r})}\left(1+\frac{1}{\cos^2(\varphi'_{mn_i}-\varphi'_{mn_r})}\right) \tag{6}$$

Transmission loss occurs at both the entry and the exit faces and is more serious at the exit face. The calculation shows that lenses with shorter focal lengths tend to suffer from greater transmission losses. For example, Fig. 4 shows that an FR0.35 (i.e. focal ratio = 0.35, see Fig. 1 for the focal ratio definition) lens has an overall transmission loss of about 22% (loss at the lens edge reaches as high as 35%), while an FR1.20 lens has an overall transmittance loss of less than 17% (with less than 18% loss at the lens edge).

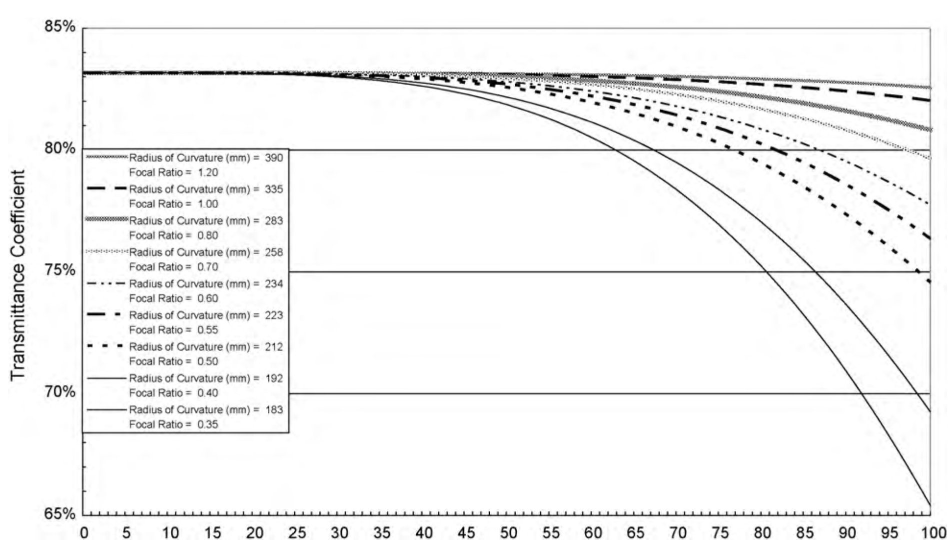


Fig. 4. The transmittance coefficient of normal incidence as functions of facet position for Fresnel lenses with focal ratios range from 0.35 to 1.20. Maximum transmission goes to the FR1.20 elliptical-based lens.

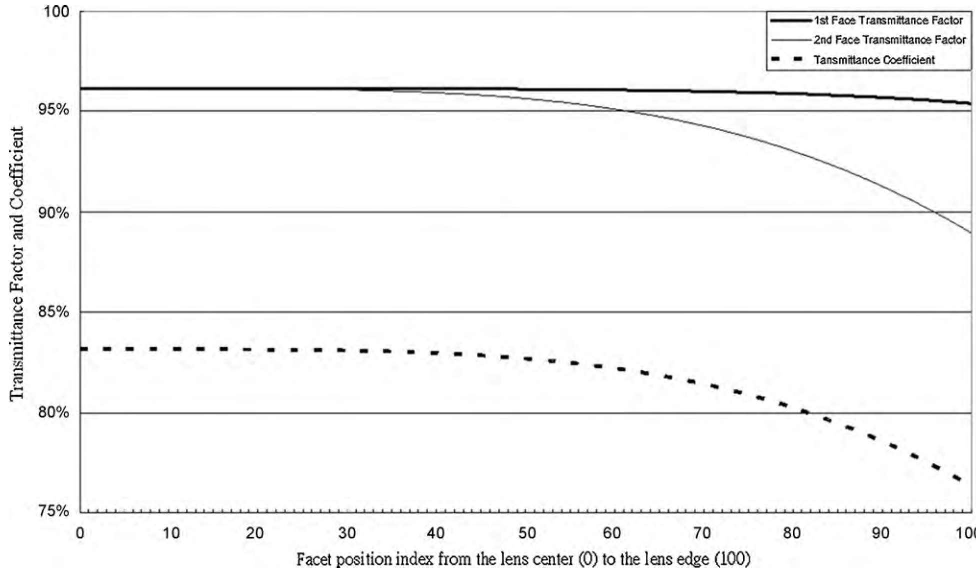


Fig. 5. The transmittance coefficients T_{mn} (calculated as per Eq. (4)) along with the transmittance factors for the first and the second prism faces (T_{mn_1} and T_{mn_2}) as functions of facet position on an FR0.55 lens, normal incidence. For a non-minimum deviation lens, T_{mn_1} and T_{mn_2} deviate more and more toward the lens edge.

Figs. 5 and 6 illustrate the entry and the exit face transmission factors along with the overall transmittance coefficient of an FR0.55 and an FR1.20 lens, respectively.

There exists a condition for a prism to have *minimum deviation* which occurs when the incoming radiation's entry face incident angle (φ_i) equals the exit face refraction angle (φ'_r). A minimum deviation prism has maximum transmission. In such a prism, a small change in the prism angles or prism positioning will only have a minimum effect on the turning angle of the light refracted from that prism. Therefore, in addition to the obvious importance of the maximum transmission, errors in the construction of systems are minimized and the focusing capability of the lens is maximized. The knowledge has been used in the design of prism spectrometers for years. A comparison of Figs. 4–6 shows that an FR1.20 elliptical-based lens comes closest to the condition of minimum deviation.

Fig. 7 demonstrates a comparison of facet angles (θ) as functions of facet position on assorted Fresnel lenses with focal ratios from 0.35 (focal length = 223 mm) to 1.20 (focal length = 390 mm). The figure shows that the facet angles of all designs increase sub-linearly. A lens that is more compact would need greater facet angles to achieve higher refraction.

Figs. 8 and 9 show the magnitudes of θ, φ_i and φ'_r as functions of facet position on an FR0.55 lens and an FR1.20 lens, respectively. For both 200-facet lenses, φ_i and φ'_r increase semi-linearly as the facet position moves toward the lens edge. On a non-minimum deviation lens, as the facet position approaches the lens edge, the deviation between φ_i and φ'_r becomes greater (Fig. 8). On a

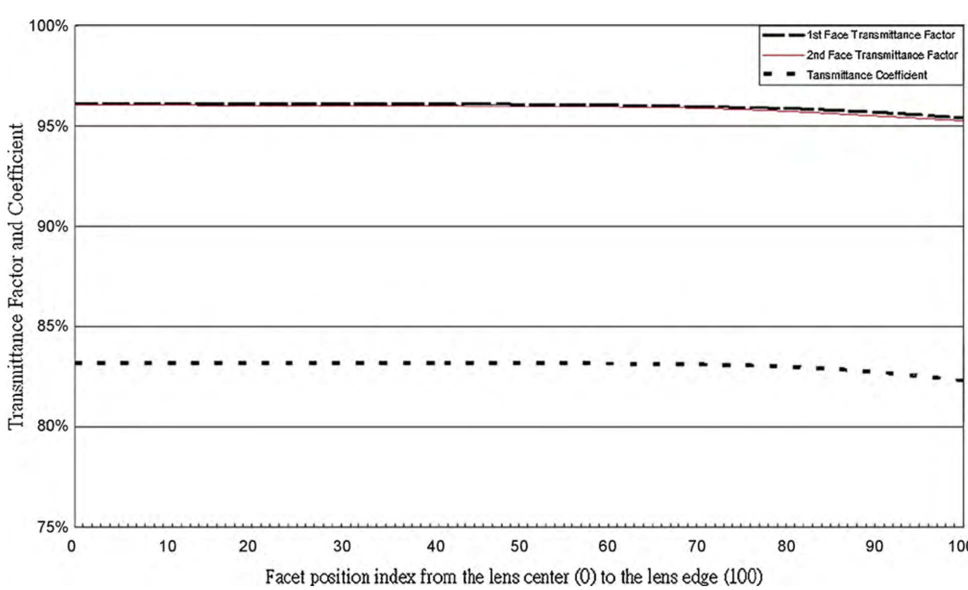


Fig. 6. The transmittance coefficients T_{mn} along with the transmittance factors T_{mn_1} and T_{mn_2} of normal incidence as functions of facet position on a minimum deviation FR1.20 lens. Note that T_{mn_1} and T_{mn_2} matches closely across the lens.

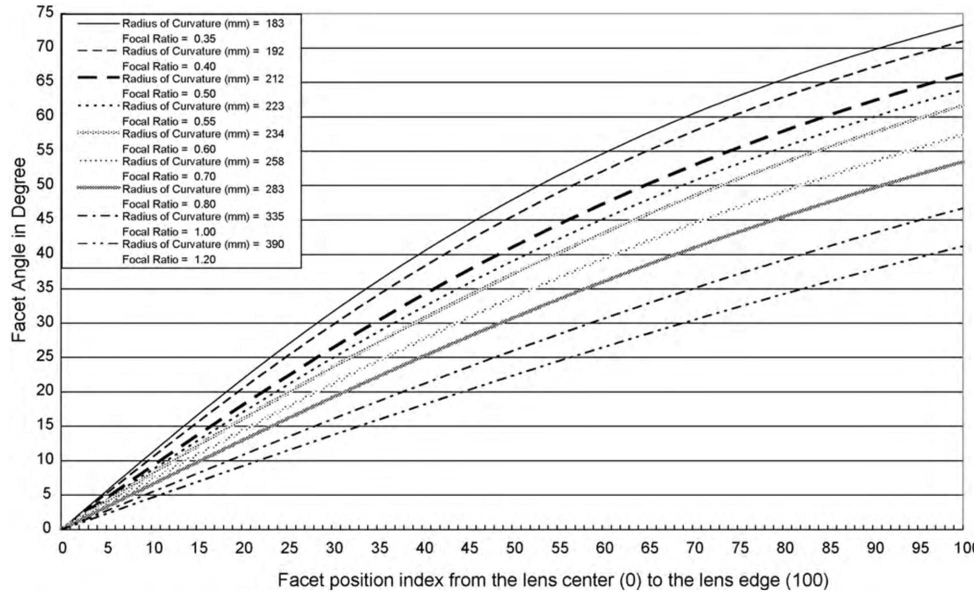


Fig. 7. A comparison of facet angles (θ) as functions of facet position on Fresnel lenses with focal ratios range from 0.35 to 1.20.

minimum deviation lens, contrastingly, the magnitudes of φ_i and φ'_r stay equal for all facets (Fig. 9).

3. Tracing the spectrum

In addition to deriving the transmission factor and coefficient of each facet at each wavelength interval, the model takes the input that includes the lens aperture; the number of facets on lens; and the focal ratio, then uses optical ray-tracing technique to calculate the concentration ratio as a function of the position on the focal plane via double summation over each facet and each designated wavelength interval:

$$W = \sum_{n=1}^{N}\sum_{m=1}^{M} E_{mn} T_{mn} \cos\varphi'_{mn_r} \tag{7}$$

In Fig. 10, the flux profile derived from the model adjusted with loss factors is compared to the measured data [22] and the flux profile derived from the previous model.

Table 1 displays the air mass 1.5 (AM1.5) solar spectrum [23] as divided into nine consecutive spectrum sectors (i.e. wavelength intervals). The *weight factor* (i.e. the percentage weight of each sector as the fraction of total sun light) is calculated from the solar spectral distribution at AM1.5. The table also lists, corresponding to each spectrum sector, acrylic's wavelength dependent *transmission factor* [24].

Any wavelength can be designated as the lens's design wavelength. And the refractive index ($\tilde{n}_n$) that corresponds to the design wavelength is called design index, $\tilde{n}_D$. The magnitude of η can be adjusted via the selection of design index (see Eq. (2)) so as to selectively block either the shorter or the longer wavelength intervals of the incoming solar irradiance. The spectrum distribution on the target area can be manipulated via such adjustment. For

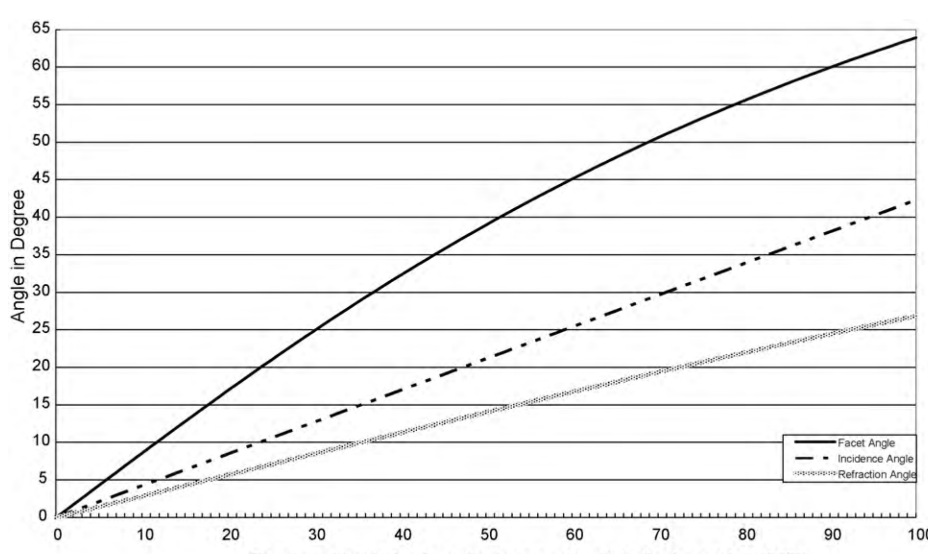


Fig. 8. The magnitudes of facet angle (θ), entry face incident angle (φ_i) and exit face refractive angle (φ'_r) as functions of facet position on a 200-facet FR0.55 Fresnel lens (focal length = 223 mm).

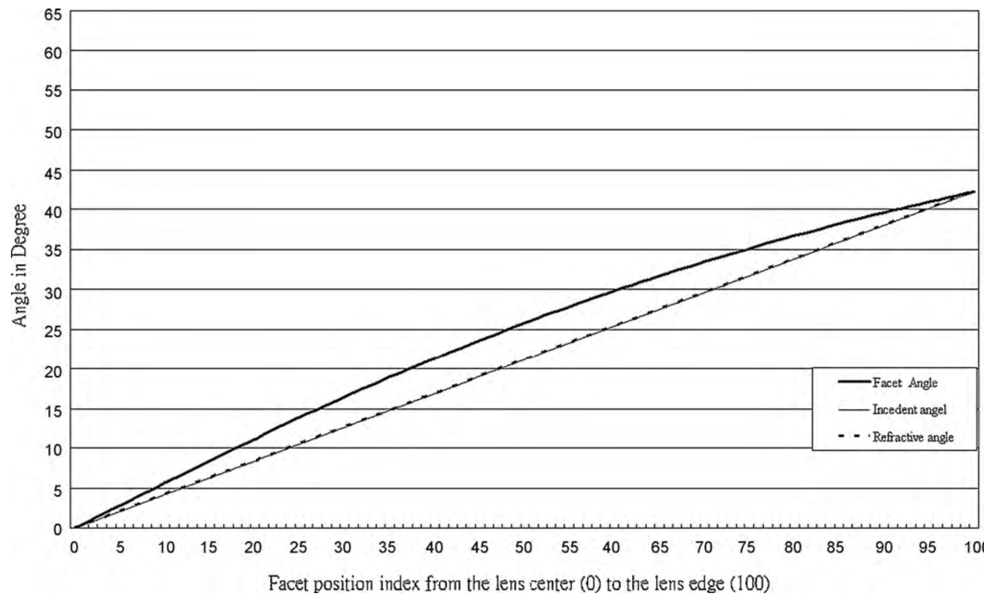


Fig. 9. The magnitudes of facet angle (θ), entry face incident angle (φ_i) and exit face refractive angle (φ_r') as functions of facet position on a 200-facet FR1.20 Fresnel lens (focal length = 390 mm).

Table 1
Spectral parameters of the solar radiation and the acrylic material.[a]

Wavelength (Å)		Color	Weight factor	Polymethylmetacrylate (acrylic)[b]	
Spectrum sector	Sector center			Refractive indices	Bulk transmission factor (T_b)
2950–4000	3480	Ultraviolet	2.67%	1.525	0.68
4000–4500	4150	Violet	2.75%	1.5155	0.97
4500–5100	4800	Blue	9.38%	1.4982	0.97
5100–5700	5400	Green	9.64%	1.4942	0.97
5700–6000	5850	Yellow	4.73%	1.4918	0.97
6000–6300	6150	Orange	4.73%	1.4906	0.97
6300–7800	6750	Red	20.59%	1.4876	0.97
7800–9900	8600	Near infrared	17.91%	1.4854	0.97
9900–22,000	11,350	Infrared	25.12%	1.4812[c]	0.82

[a] Derived from Fig. 14.
[b] Sample thickness = 3.2 mm.
[c] Estimated value via Harmann's formula, all formulas that present the index of refraction as a function of a wavelength of electromagnetic radiation, also called dispersion equation, Cauchy formula, or Hartmann formula.

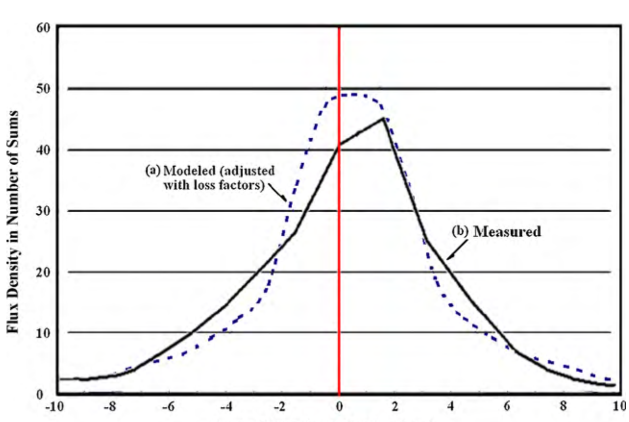


Fig. 10. A comparison of (a) the modeled flux profile adjusted with lose factors, and (b) the measured relative radiation flux [24]. Note that the measured curve appears shifted due to mis-orientation. To simulate the effect of such mis-orientation, the modeled flux profile is taken from the incidence coming in at the angle of 4.25° to the left of the lens axis.

example, a lens designed for the shorter wavelength interval has greater η and is less friendly to the longer wavelength intervals.

Fig. 11 shows the spectrum distribution on the receiver under a lens designed for the violet sector centered at 4150 Å. In the solar spectrum, violet sector weights only about 2.75% while infrared and near infrared sectors (7800 Å and above) jointly weight about 43%. In the target center of such a lens, however, violet manages to peak at the intensity of approximately three suns and plays a much more significant role (weight over 23% vs. near infrared and infrared's combined weight of 25%). A great portion of the infrared sector is scattered, blocked, or refracted off the receiver. Note that the colors with wavelength longer than violet tend to be under refracted and form a dip in the center of their respective profiles.

Blue light weights 9.4% in the solar spectrum. When using 4800 Å (center wavelength of the blue sector) as the design wavelength, blue light manages to peak at about nine suns in its profile center (see Fig. 12). The neighboring wavelengths that include violet and green also accumulate nicely at the target center. Colors in the longer wavelength range (especially for red and infrared) are still under refracted and have dented profile

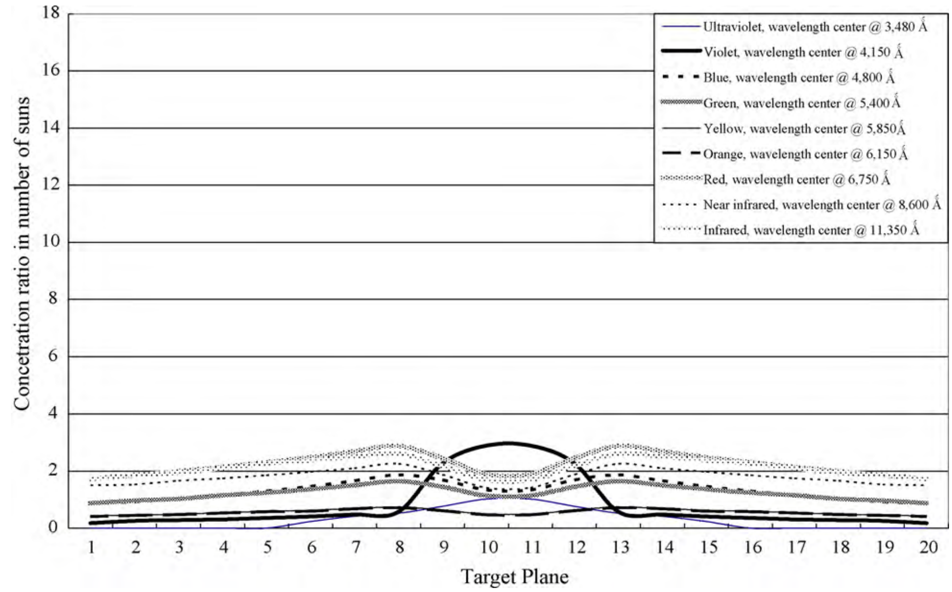


Fig. 11. Flux density of various wavelength intervals on the absorber under a lens with a design index of 1.5155. This design index has a corresponding wavelength interval between 4000 and 4500 Å (centered at 4150 Å, which is violet). The absorber is divided into 20 strips. The graph represents the respective amount of energy in each spectrum sector in number of suns.

centers. The flux profiles of orange, yellow, and green are flat on the top.

When red (centered at 6750 Å) is designated as the design wavelength (Fig. 13), the blue light sector in the target center dims significantly (compared to Fig. 12). Red, along with its neighboring colors (such as orange, yellow, and green) concentrates nicely. Every spectrum sector but infrared, which is the most significant part of the solar spectrum, forms normal peak profiles. This design produces the best optical efficiency among all designs examined.

In the photovoltaic application, a solar cell's capacity to generate photocurrent from a given wavelength is measured by its quantum efficiency. The maximum photocurrent (I_{max}) available is:

$$I_{max} = \sum_{n=1}^{N} Qe_n W_n \quad (8)$$

where Qe_n is the cell's quantum efficiency with respect to the n^{th} wavelength interval and W_n is the total energy of the n^{th} wavelength interval available to the cell.

The spectral response of any type of solar cells is not uniform. For example, the multi-junction cell illustrated in the bottom chart in Fig. 14 does not respond to wavelength beyond 17,000 Å [25]. This wavelength interval constitutes about 5% of the solar spectrum. It tends to generate heat and is not desirable for photovoltaic purpose. It means a significant heat reduction if a lens can be designed to block, scatter, or refract this heat-generating sector off the receiver. The reduction of heat will enhance the cell efficiency. Another way to achieve the same goal, which may be an easier solution, is to apply a filter that will keep that part of the spectrum from entering the lens.

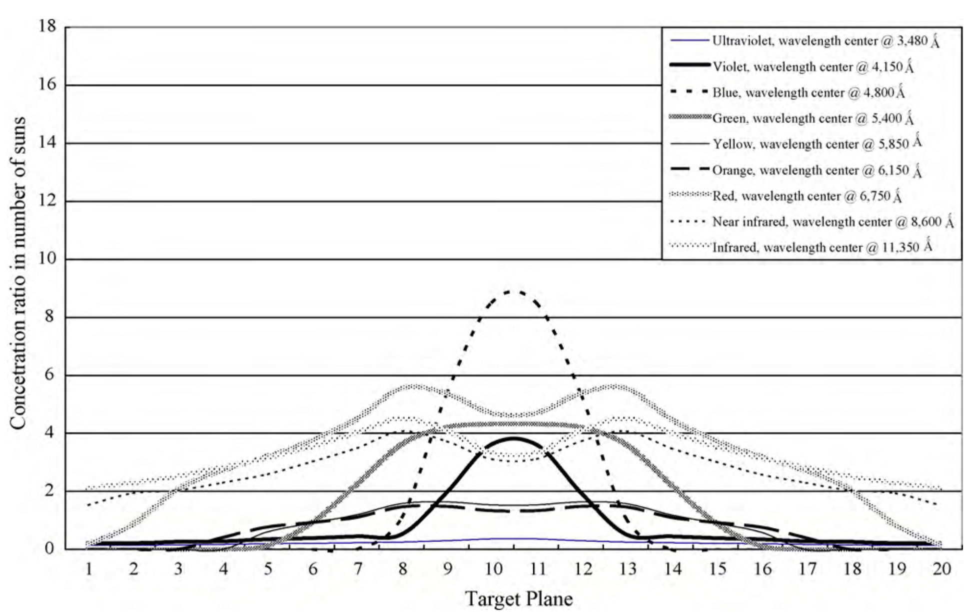


Fig. 12. Flux density of various spectrum sectors on the absorber under the lenses with design index of 1.4982. This design index has a corresponding wavelength interval between 4500 and 5100 Å (centered at 4800 Å, which is blue).

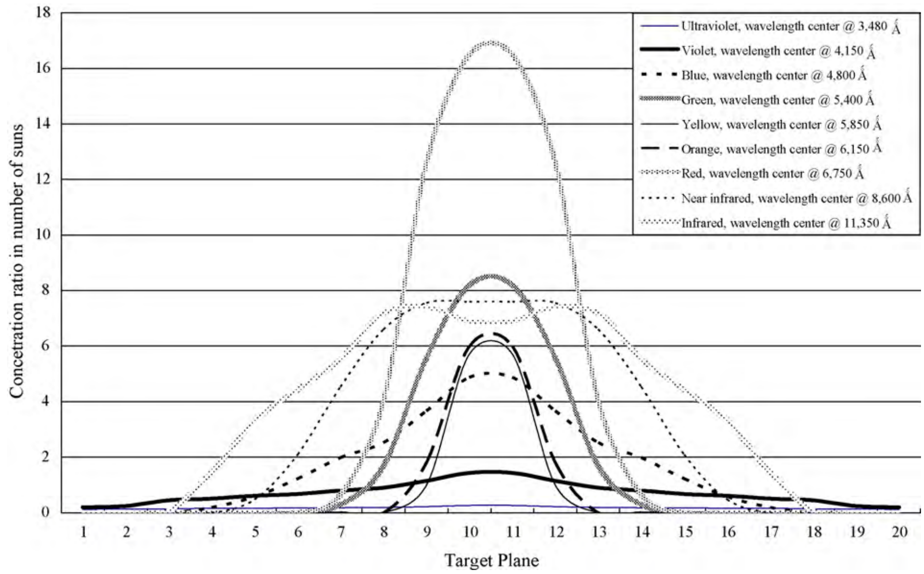


Fig. 13. Flux density of various spectrum sectors on the absorber under the lens with design index of 1.4886. This design index has a corresponding wavelength interval between 6300 and 7800 Å (centered at 6750 Å, which is red).

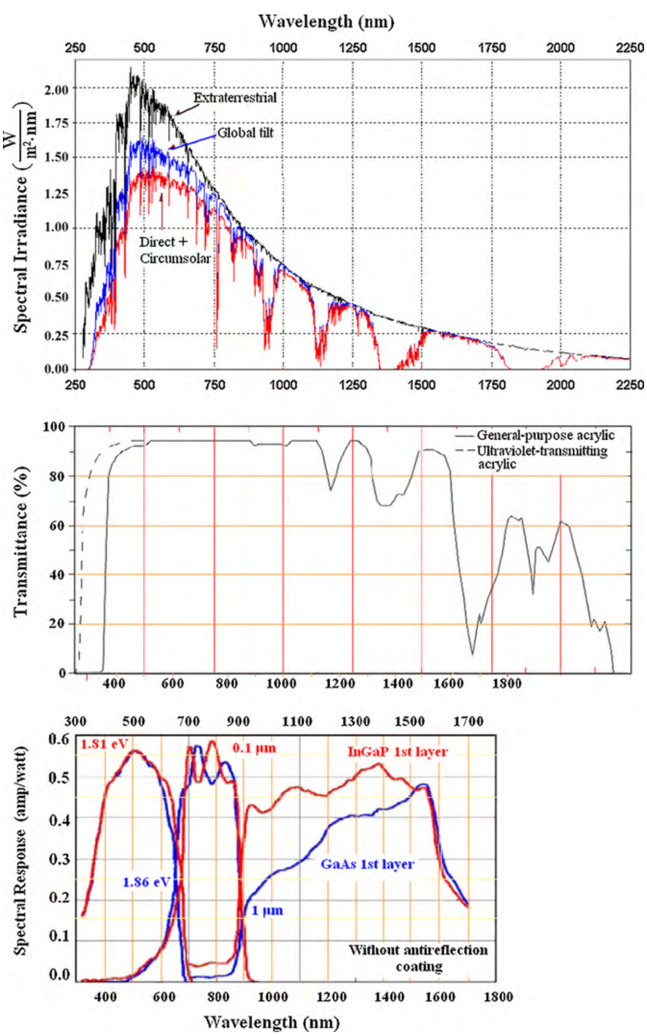


Fig. 14. Top [23]: measured spectral irradiance, where extraterrestrial indicates the solar spectrum at air mass zero (AM0), "direct" indicates direct normal spectral irradiance, and "global tilt" indicates global total spectral irradiance (direct plus scattered) on the 37° sun facing tilted surface. Both global tilt and direct are defined at AM 1.5. Middle [24]: transmittance of general purpose acrylic (straight line) and ultraviolet transmitting acrylic (dashed line). Bottom [25]: the spectral response of the third generation InGaP/InGaAs/Ge 3-junction concentrator solar cell (as distinguished to the first generation crystalline silicon solar cells and second generation thin-film solar cells). All three charts are lined up in wavelength.

4. Conclusion

Via loss tracking and wavelength oriented ray tracing, this research has investigated the loss inherent in a Fresnel lens as well as the contribution of each wavelength interval to the flux profile on the absorber of a Fresnel lens solar concentrator system.

Besides examining the loss factors that include TIR, facet blocking, surface reflectance as well as scattering due to groove defects and distorted lens material; this paper has quantified the transmittance loss and prism-tip scattering loss. For a non-minimum deviation lens, as the incident angle increases, the rate of loss at the exit face increases more rapidly than it does at the entry face. As such, the deviation of these two losses becomes more apparent. The paper has identified that, an FR1.20 elliptical-based lens comes closest to the condition of minimum deviation and closely duplicate the curvature required to achieve maximum transmission. For such a lens, the rate of transmission loss at both faces stay minimal and equal as the incident angle increases. For the lenses with FR less than 1.20, more transmission loss occurs at the exit face than at the entry face of the serration.

After being adjusted with loss factors the model become more realistic and is able to derive a more accurate flux profile comparing to the measured data and to the flux profile derived from the numerical model [22].

In addition, this research demonstrates that the design wavelength of a Fresnel lens decides which part of the spectrum becomes the most concentrated in the target center. Also, the magnitude of side angle, η, can be adjusted via the selection of design index so as to selectively block some part of either the shorter or the longer spectrum sectors of the incoming solar irradiance. All these help to manipulate the *spectrum* distribution on the target area under the Fresnel lens concentrator.

As some wavelengths are more fertile than the rest in photon to photocurrent conversion, the lens should be designed to gather on the target cell the photon flux that generates the most photocurrent. Such deign usually do not produce maximum optical efficiency.

References

[1] Cosby R. Performance, manufacture, and protection of large cylindrical Fresnel lenses for solar collection. Final report. Ball State University, Marshall Space Flight Center, NCA8-00103, Mod. No. 2; 1975.

[2] Hastings L, Allums S, Cosby R. An analytical and experimental evaluation of Fresnel lens solar concentrator. NASA TM-73333; 1976.

[3] Hastings L, Allums S, Jensen W. An analytical and experimental investigation of a 1.8 by 3.7 Fresnel lens solar concentrator. In: ISES-America Sec. conference proceeding; 1977.

[4] James LW, Williams JK. Fresnel optics for solar on photovoltaic cells. In: 13th IEEE photovoltaic specialist conference. 1978. p. 673.

[5] O'Neill MJ, Waller RA. Analytical/experimental study of the optical performance of a transmittance-optimized linear Fresnel lens solar concentrator. In: ISES-American section. Proc., annual meeting; 1980.

[6] O'Neill MJ. Solar concentrator and energy collection system. United States Patent 4069812; 1978.

[7] Kritchman EM, Friesem AA, Yekutieli G. Efficient Fresnel lens for solar concentration. Solar Energy 1979;22:119–23.

[8] Kritchman EM, Friesem AA, Yekutieli G. Highly concentrating Fresnel lenses. Appl Opt 1979;18(15):2688–95.

[9] Winston R. Principles of solar concentrators of a novel design. Solar Energy 1974;16:89–95.

[10] Rabl A. Optical and thermal properties of compound parabolic concentrators. Solar Energy 1976;18:479–511.

[11] Cosby R. The linear Fresnel lens: solar optical analysis of error effects. In: SESQ2 – America section proceedings; 1977. p. 35-14–35-18.

[12] Collares-Pereira M. High temperature solar collector with optimal concentration: non-focusing Fresnel lens with secondary concentrator. Solar Energy 1979;23:409–20.

[13] Collares-Pereira M, Rabl A, Winston R. Lens-mirror combinations with maximal concentration. Appl Opt 1977;16(10):2677–83.

[14] Lorenzo E, Luque A. Fresnel lens analysis for solar energy applications. Appl Opt 1981;20(17):2941–5.

[15] Lorenzo E, Luque A. Comparison of Fresnel lenses and parabolic mirrors as solar energy concentrators. Appl Opt 1982;21(10):1851–3.

[16] Lorenzo E. Chromatic aberration effect on solar energy systems using Fresnel lenses. Appl Opt 1981;20(21):3729–32.

[17] Leutz R, Suzuki A, Akisawa A, Kashiwagi T. Design of a non-imaging Fresnel lens for solar concentrators. Solar Energy 1999;65(6):379–88.

[18] Yeh N. Optical geometry approach for elliptical Fresnel lens design and chromatic aberration. Solar Energy Mater Solar Cells 2009;93(8):1309–17.

[19] Leutz R, Suzuki A, Akisawa A, Kashiwagi T. Nonimaging Fresnel lens concentrator – the prototype. In: Proceedings, 1st Int's power & energy Conf; 1999.

[20] Leutz R, Suzuki A. Nonimaging Fresnel lenses: design and performance of solar concentrators. Berlin (Heidelberg/New York): Springer; 2001.

[21] Yeh N. Optical geometry approach for computerized design of Fresnel lens solar concentrator. Mingdao J 2007;3(1):33–50.

[22] Leutz R, Suzuki A, Akisawa A, Kashiwagi T. Shaped nonimaging Fresnel lenses. Journal Opt A Pure Appl Opt 2000;2:112–6.

[23] ASTM. Standard tables for reference solar spectral irradiances: direct normal and hemi-spherical on 37° tilted surface. Book of standards, vol. 14.04. ASTM G173-03e1; 2003.

[24] Fresnel Technologies, Inc. Fresnel lenses. Available from: http://www.fresnel-tech.com/pdf/FresnelLenses.pdf [accessed 09.02.10].

[25] Yamaguchi M, Takamoto T, Araki K, Ekins-Daukes N. Multi-junction III–V Solar cells: current status and future potential. Solar Energy 2005;79:78–85.